High-loading individually dispersed $NiCo_2O_4$ anchoring on Checkerboard-like C/CNT Nanosheets as binder-free high rate electrode for lithium storage

Hanwei Wang[1†], Lintong Hu[2†], Chao Wang[1], Qingfeng Sun[1*], Huiqiao Li[2*], Tianyou Zhai[2]

[1]School of Engineering, Zhejiang A&F University, Hangzhou 311300, China.

[2]State Key Laboratory of Materials Processing and Die & Mould Technology, School of Materials Science and Engineering, Huazhong University of Science and Technology (HUST), Wuhan 430074, China

[†]These authors contributed equally to this work.

[*]Corresponding author: Qingfeng Sun (qfsun@zafu.edu.cn) and Huiqiao Li (hqli@hust.edu.cn)

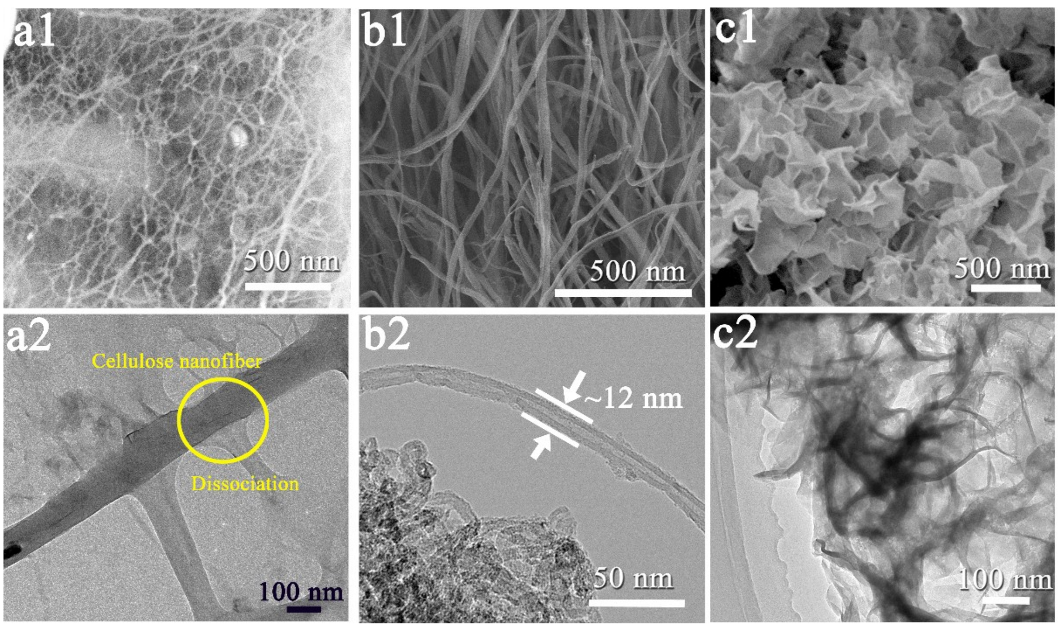

Fig. S1. SEM and TEM images of (a) pure cellulose 2D-network, (b) pure CNTs and (c) original $NiCo_2O_4$.

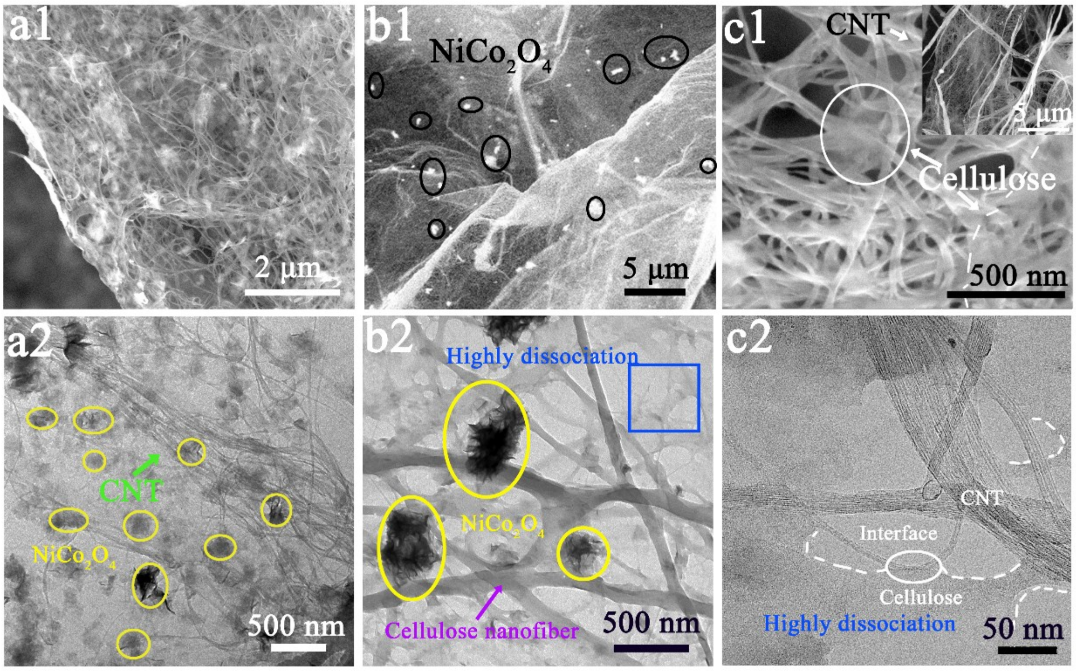

Fig. S2. SEM and TEM images of (a) $NiCo_2O_4$@cellulose/CNT nanosheets, (b) $NiCo_2O_4$@cellulose and (c) CNT@cellulose.

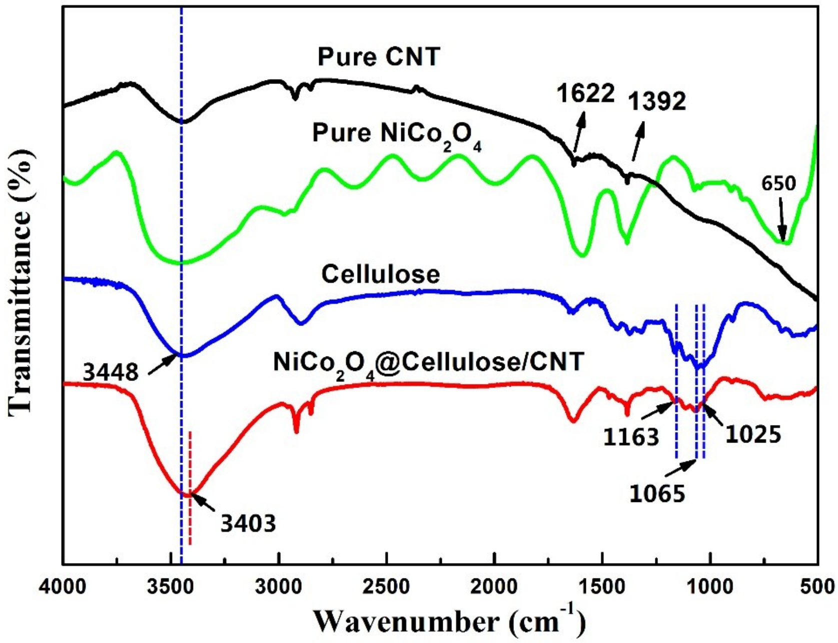

Fig. S3. FTIR spectra of pure CNT, pure $NiCo_2O_4$, pure cellulose and $NiCo_2O_4$@cellulose/CNT nanosheets. As for the pure CNT, the observed two peaks at 1622 and 1392 cm^{-1} correspond to the antisymmetric stretching and symmetric stretching of COO^-, indicating the existence of carboxyl groups on the surface of carbon. The same peaks also are observed in pure $NiCo_2O_4$, which may be provided by the adsorbed $C_2O_4^{2-}$ (raw material) or the $-COO^-$. The existence of carboxyl groups and oxygen atom on the surface of CNT and $NiCo_2O_4$ provide the foundation for the formation of the hydrogen bond to the polyhydroxy cellulose, leading to the shifting of –OH bond from 3448 cm^{-1} of cellulose to the 3403 cm^{-1} of $NiCo_2O_4$@cellulose/CNT.

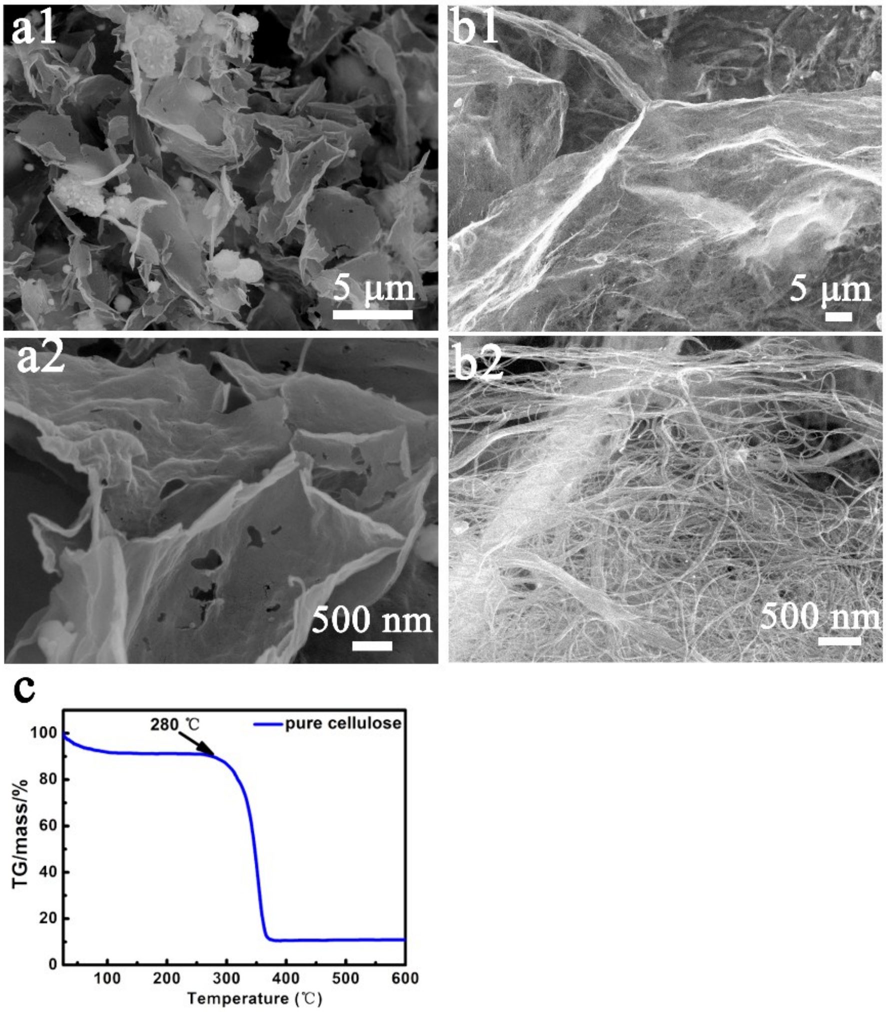

Fig. S4. SEM images of (a) cellulose-derived carbon nanosheets and (b) C/CNT nanosheets; (c) TG curve of the pure cellulose under Ar atmosphere. After pyrolysis process, the mass of cellulose only retained 10.75%, representing to the carbon content.

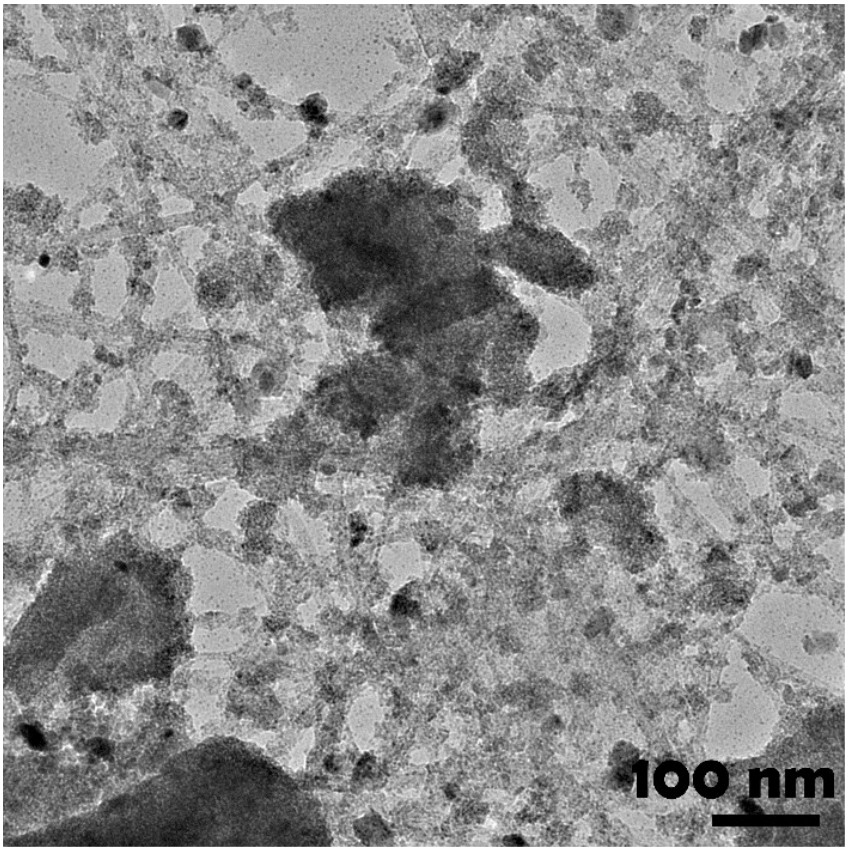

Fig. S5. TEM images of $NiCo_2O_4$/CNT.

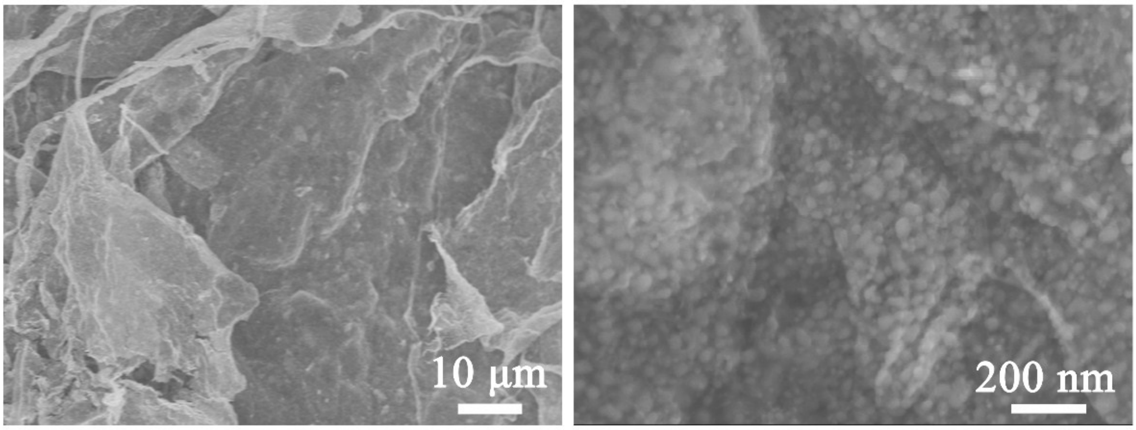

Fig. S6. SEM images of N@C/CNT-89.1.

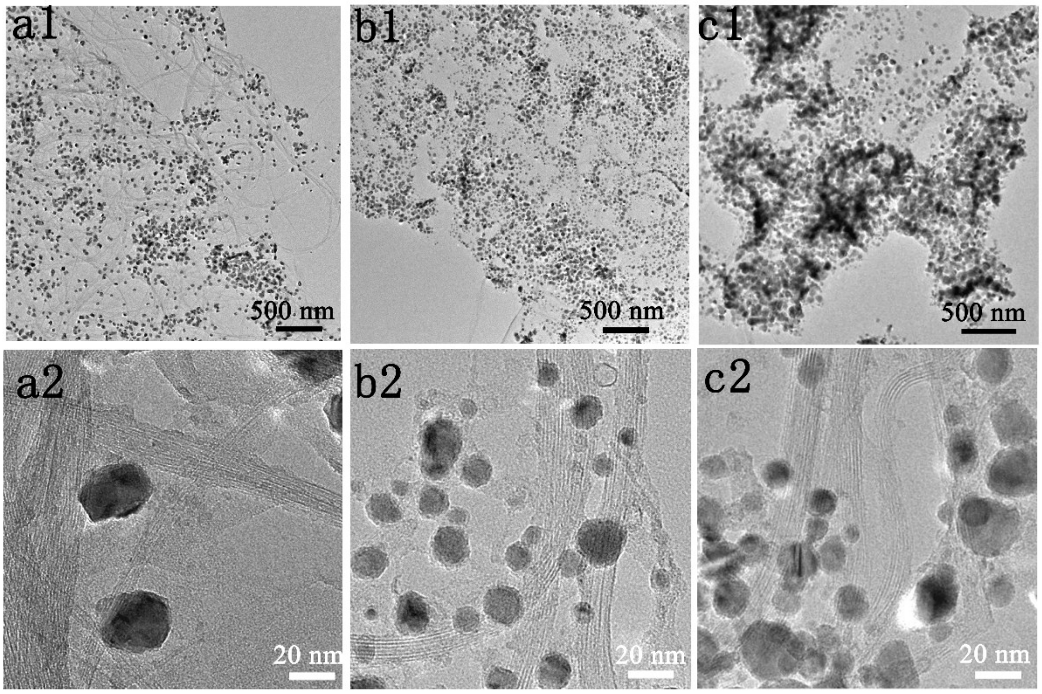

Fig. S7. TEM images of (a) N@C/CNT-61.4, (b) N@C/CNT-77.6 and (c) N@C/CNT-89.1.

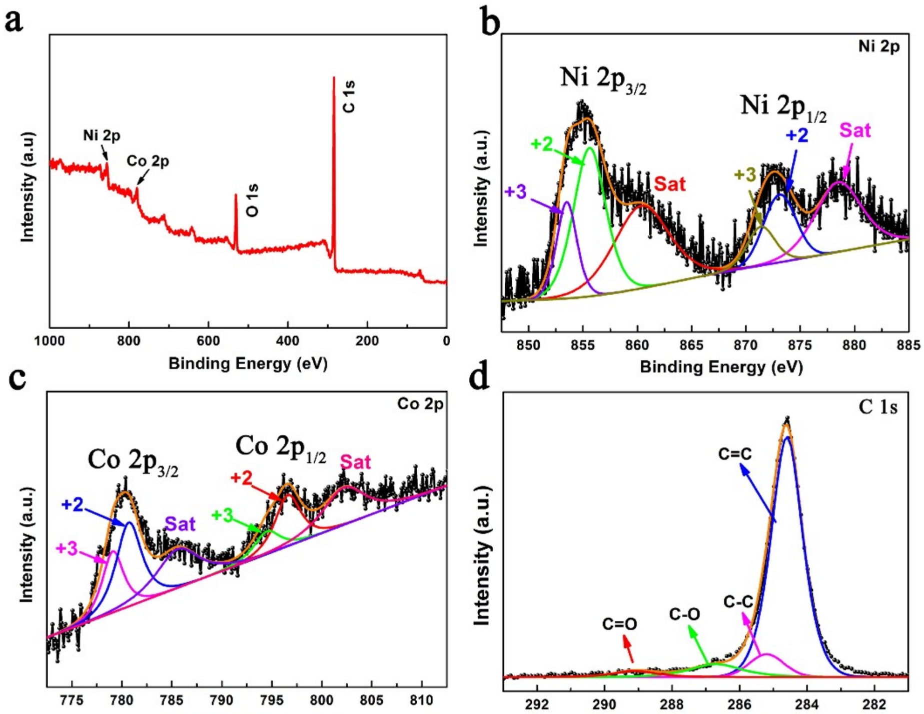

Fig. S8. (a) Survey spectrum, (b) Ni2p, (c) Co2p, and (d) C1s spectra of N@C/CNT-

85.1.

As shown in **Fig. S8a,** the two typical characteristic peaks at 856.9 and 874.3 eV in the Ni 2p emission spectrum were corresponding to the two spin-orbit doublets of Ni $2p_{1/2}$ and Ni $2p_{3/2}$. It could be fitted with the six Gauss peaks, 853.6 and 871.4 eV corresponded to the Ni $2p_{3/2}$ and Ni $2p_{1/2}$ in Ni^{3+}, 855.5 and 873.2 eV indexed to the Ni $2p_{3/2}$ and Ni $2p_{1/2}$ in Ni^{2+}, and 860.6 and 878.7 eV were the satellite peaks. Similarly, the two states of the Co were observed in Co 2p emission spectrum (**Fig. S8b**). The peaks at 779.2 and 794.5 eV were attributed to the Co^{3+}. The other peaks at 780.7 and 796.3 eV were indexed to the Co^{2+}. The results of XPS indicated the coexistence of Co^{2+}/Co^{3+} and Ni^{2+}/Ni^{3+} in N@C/CNTs, which conformed to the components of $NiCo_2O_4$ in previously reports. **Fig. S8c** displayed the C 1s emission spectrum of the N@C/CNT-85.1, which could be fitted to four peaks centered at 284.6, 285.2, 286.7 and 289.1 eV, corresponding to the C=C, C-C, C-O and C=O groups, respectively. The largest C=C peak indicated highly graphitization of carbon that was mainly provided by CNTs.

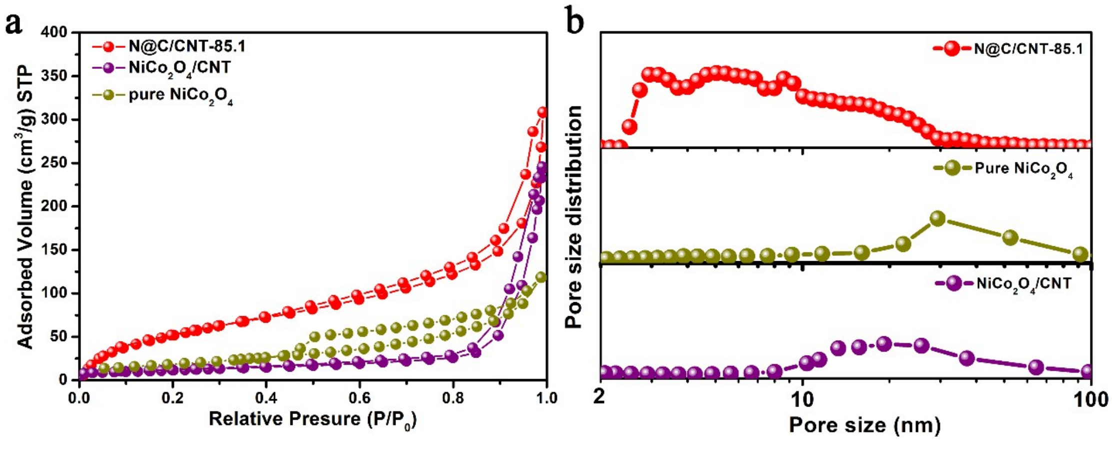

Fig. S9. (a) N_2 adsorption-desorption isotherms and (b) pore size distributions of the

N@C/CNT-85.1, pure $NiCo_2O_4$ and $NiCo_2O_4$/CNT.

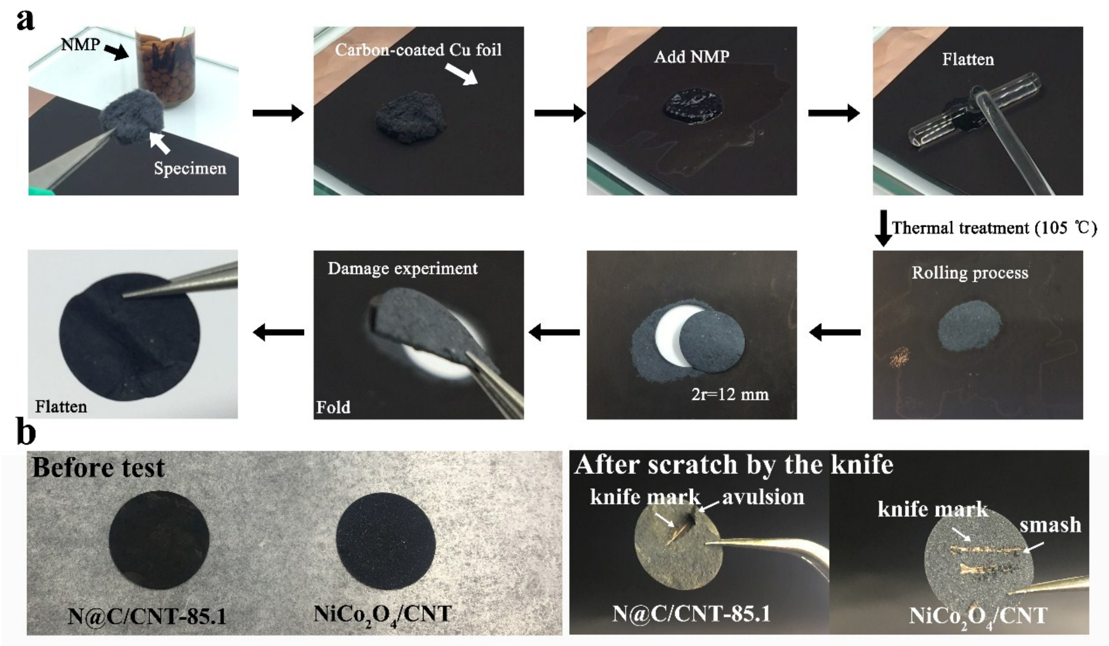

Fig. S10. Preparation processes of the binder-free N@C/CNTs electrode. The size, morphology and mass of the N@C/CNTs aerogels can be **controlled easily** in freeze-drying and carbonization processes. Here, we used a low mass specimen (~5 mg) to demonstrate this preparation processes of the binder-free electrode. The obtained binder-free electrode possess a strong adhesion with the carbon-coated Cu foil. Even after the damage experiment, the sample is still firmly adhered on the surface of the substrate, which might be due to the self-assembly of the nanosheets as well as the combination of the active functional groups between the nanosheets and carbon-coated Cu foil. After the scratch test by the knife, compared to the pulverization and fall off of the $NiCo_2O_4$/CNT electrode, the N@C/CNT-85.1 electrode had a tearing cut. It confirmed the existence of the action forces between the nanosheets, suggesting it possesses a well strength as the binder-free electrode.

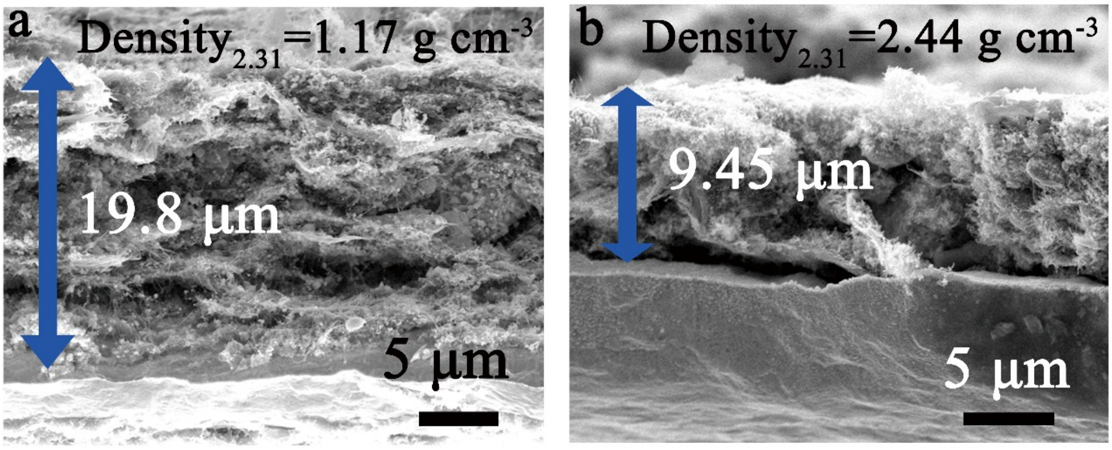

Fig. S11. SEM images of cross section of N@C/CNT-85.1 electrode (a) before and (b) after a compression disposing at the pressure of 20 MPa, when the mass loading of N@C/CNT-85.1 is 2.3 mg cm^{-2}.

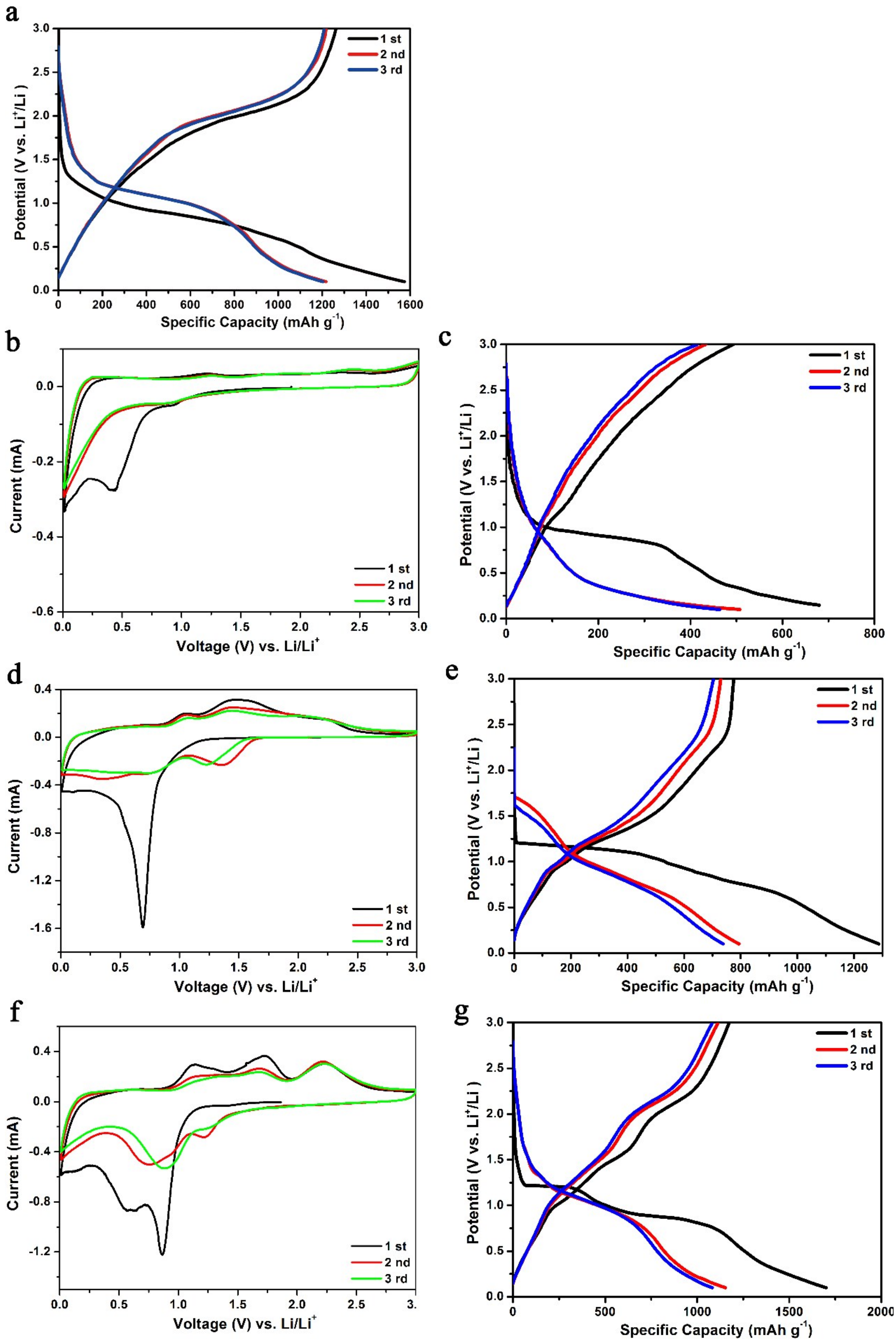

Fig. S12. The first three voltage-capacity curves of (a) N@C/CNT-85.1, (c) pure C/CNT nanosheets, (e) pure $NiCo_2O_4$ and (g) $NiCo_2O_4$/CNT at 0.1 A g^{-1} ; CV curves of (b) pure C/CNT nanosheets, (d) pure $NiCo_2O_4$ and (f) $NiCo_2O_4$/CNT at a scanning rate of 0.2 mV s^{-1} in the voltage range of 0–3.0 V.

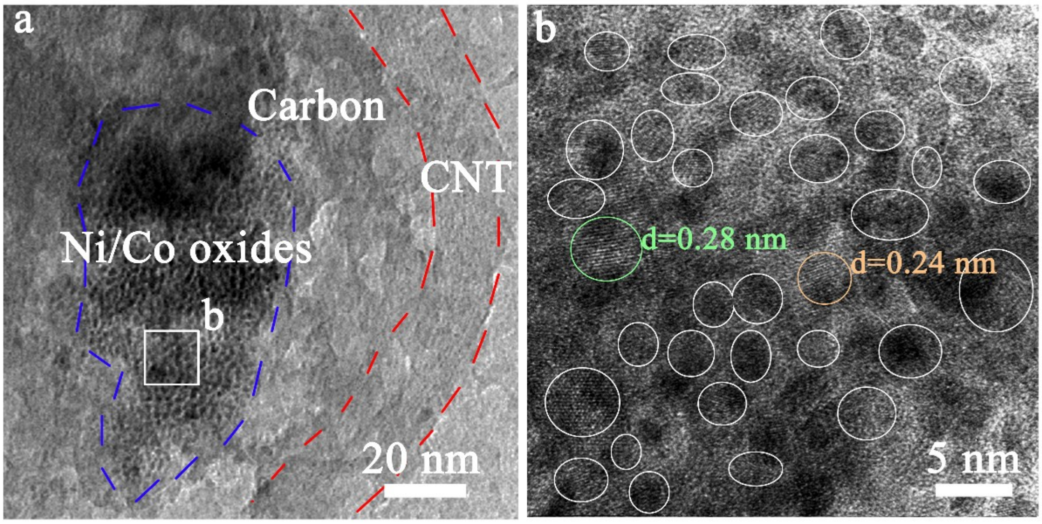

Fig. S13. The TEM images of N@C/CNT-85.1 after the rate tests. The interplanar distance of 0.28 and 0.24 nm might be contributed by the Co_3O_4 and NiO NPs.

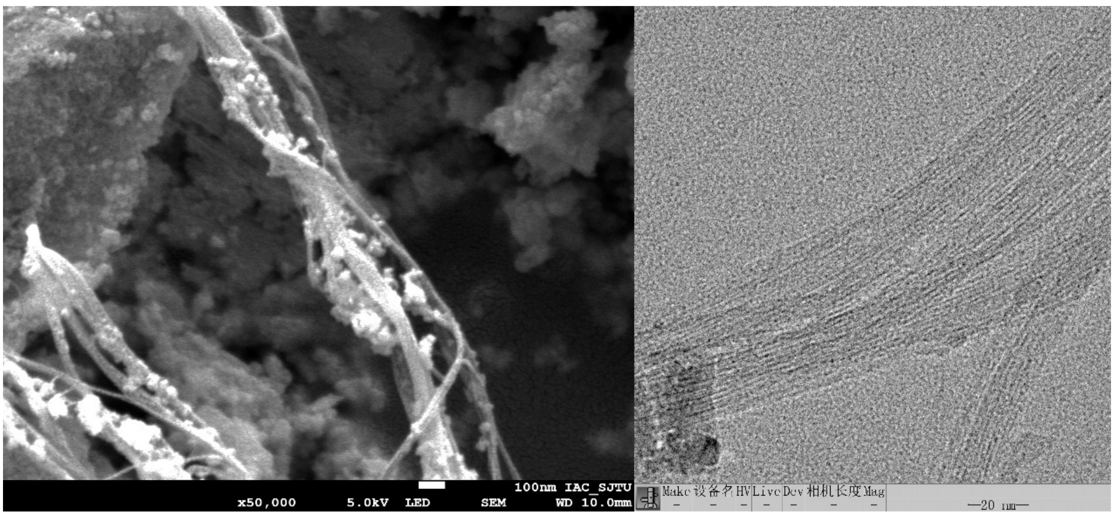

Fig. S14. The SEM and TEM images of $NiCo_2O_4$/CNT electrode after cycling.

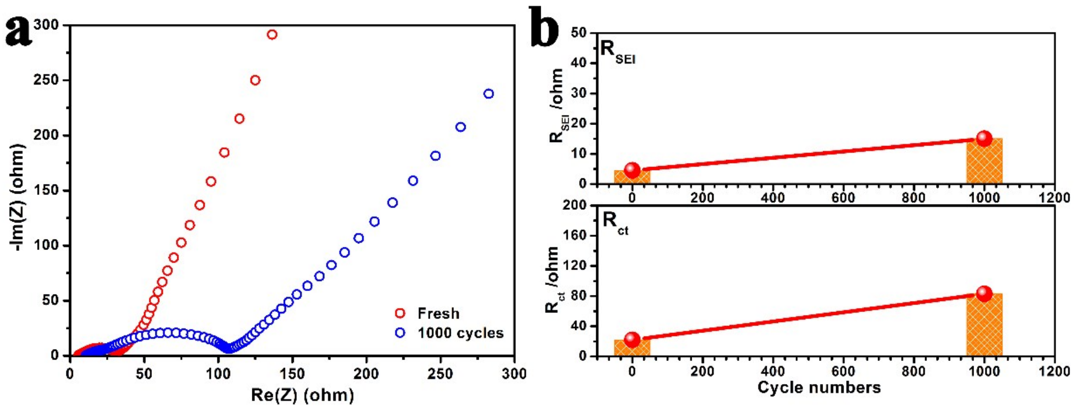

Fig. S15. (a) Nyquist plots of N@C/CNT-85.1 electrode under the mass loading of 12.8 mg cm^{-2} before and after 1000 cycles; (b) R_{SEI} and R_{ct} performance of N@C/CNT-85.1. After cycling, the values of R_{SEI} and R_{ct} in this electrode increased by just 4.3 and 56 Ω, respectively.

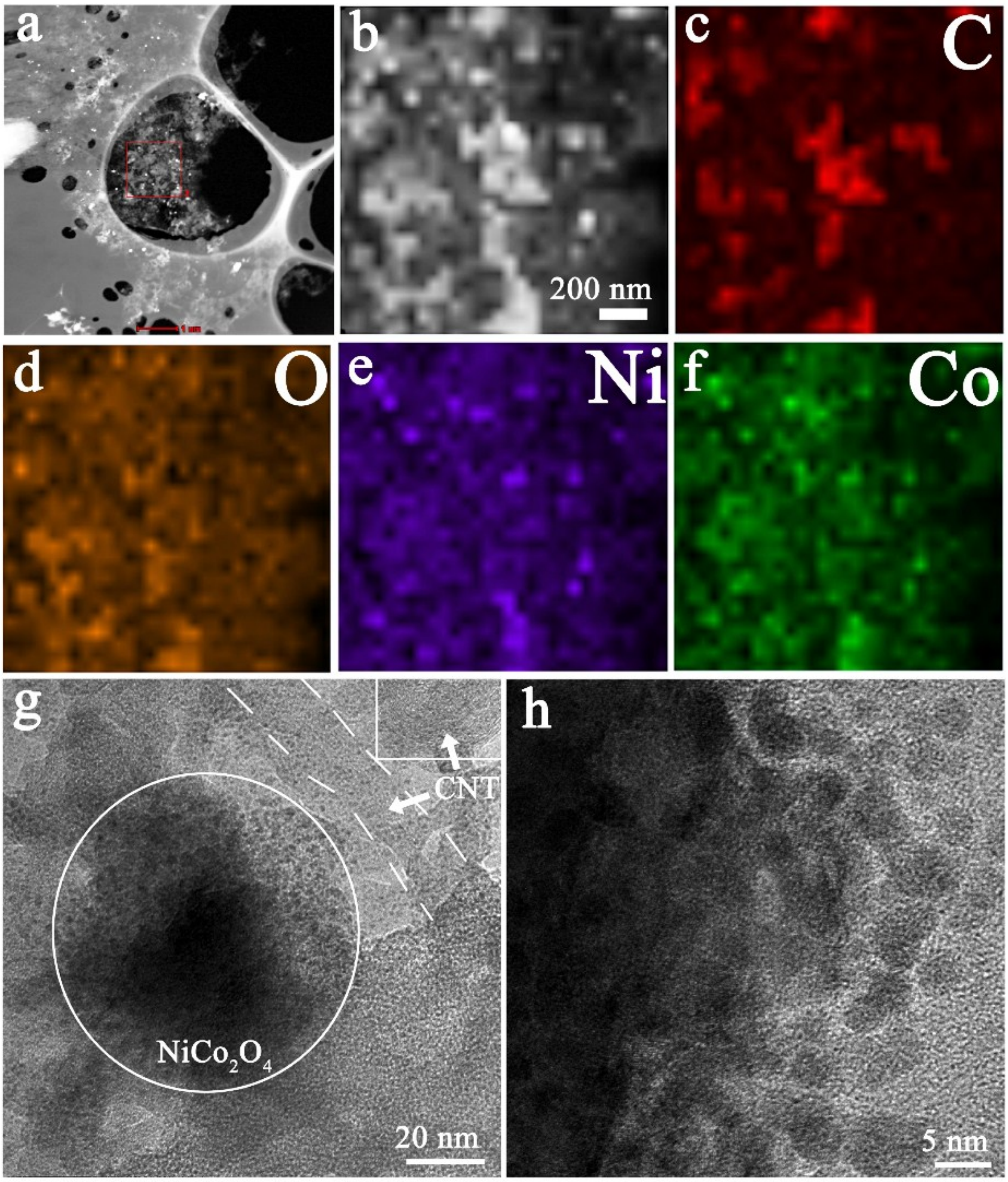

Fig. S16. N@C/CNT-85.1 after 4000 cycles: (a) HAADF-STEM image; (b-f) elemental mapping images; (g) TEM image; (h) HRTEM image.

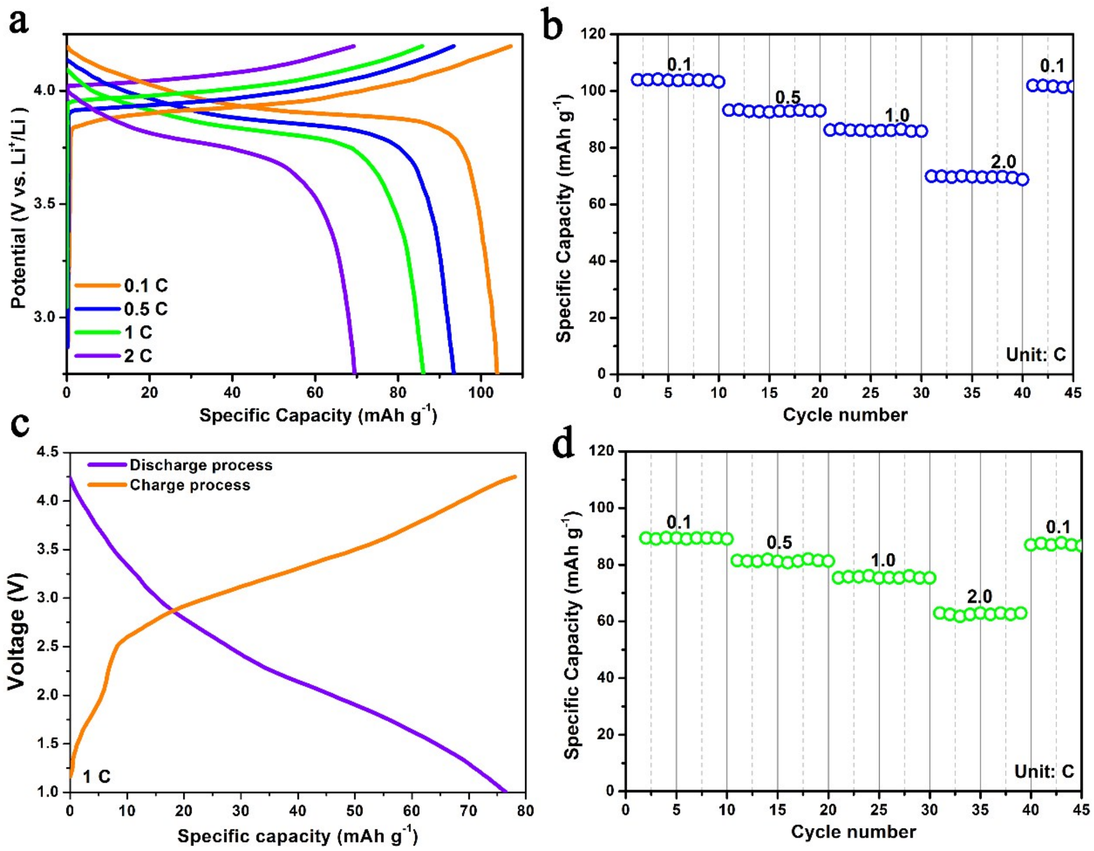

Fig. S17. Charge/discharge curves and rate performance at 0.1~2.0 C: (a) the charge/discharge voltage profile and (b) rate performance of half-cell using $LiCoO_2$ as cathode; (c) the typical charge/discharge voltage profile (the 5th cycle) and (d) rate performance of full-cell using $LiCoO_2$ as cathode and N@C/CNT-85.1 as anode. The electrochemical performances of commercial $LiCoO_2$ was assessed by half-cell in **Fig. S17a, b**, showing the capacities of 102, 92, 87, 70 mAh g^{-1} at 0.1, 0.5, 1, and 2C, respectively (1C=274 mA g^{-1}). The capacity of N@C/CNT-85.1 electrode (12.8 mg cm^{-2}) at 1 C is about 900 mAh g^{-1}. Thus, to ensure good capacity matching of the electrodes, the cathode/anode mass ratio in full-cell was ~12:1 (N/P capacity ratio of 1.08). The theoretical capacity Q_{total} calculated by the following Equation: $1/Q_{total}=1/Q_{anode}+1/Q_{cathode}$. Where Q_{anode} and $Q_{cathode}$ are the measured gravimetric capacity of anode and cathode at 1 C.

Table S1. A survey of electrochemical performances of anode in LIBs.

Description	Mass loading (mg cm^2)	TMOs contents (%)	Reversible capacity (mAh g^{-1})	Cycling stability [a] (%)	ICE[b] (%)	High rate capability (%)	Reference
N@C/CNT-85.1	1.8~2.3 mg cm^{-2}	85.1%	1208 mAh g^{-1} at 0.1 A g^{-1}	92.9% after 4000 cycles at 20 A g^{-1}	78.7%	830 mAh g^{-1} at 20 A g^{-1}	This work
Hollow-structured $NiCo_2O_4$/CNT nanocomposite		56%	1005 mAh g^{-1} at 0.2 A g^{-1}	72% after 200 cycles at 0.5 A g^{-1}	62%	643 mAh g^{-1} at 5 A g^{-1}	[1]
Urchin-like $NiCoO_2$@C nanocomposites	0.8 mg cm^{-2}	82%	1201 mAh g^{-1} at 0.4 A g^{-1}	76% after 200 cycles at 0.4 A g^{-1}	62.7%	About 300 mAh g^{-1} at 1.6 A g^{-1}	[2]
$NiCo_2O_4$@GO hybrid composite	0.65 mg cm^{-2}	85%	1046 mAh g^{-1} at 0.05 A g^{-1}	75.5% after 100 cycles at 0.1 A g^{-1}	77.6%	387 mAh g^{-1} at 4 A g^{-1}	[3]
1D porous $NiCo_2O_4$ microrods			1036 mAh g^{-1} at 0.1 A g^{-1}	75% after 600 cycles at 0.5 A g^{-1}		700.5 mAh g^{-1} at 2 A g^{-1}	[4]
$NiCo_2O_4$ nanoneedles@C	0.45 mg cm^{-2}		1005 mAh g^{-1} at 0.2 A g^{-1}	102.7% after 200 cycles at 0.1 A g^{-1}	71.38 %	Low rate capability	[5]
Yolk-shell $NiCo_2O_4$ microspheres	2-3 mg		1203 mAh g^{-1} at 0.4 A g^{-1}	98.2% after 100 cycles at 1 A g^{-1}	54.85 %	813 mAh g^{-1} at 5 A g^{-1}	[6]
$NiCo_2O_4$@ $ZnCo_2O_4$	0.9-1.1 mg cm^{-2}		1176.1 mAh g^{-1} at 0.1 A g^{-1}	107.8% after 600 cycles at 5 A g^{-1}	76.3%	950.4 mAh g^{-1} at 5 A g^{-1}	[7]
Carbon coated 3D $NiCo_2O_4$	2.1-2.3 mg	54.8%	929.46 mAh g^{-1} at 0.5 A g^{-1}	82.9% after 100 cycles at 0.5 A g^{-1}	74.3%		[8]
FeOx@ cellulose-carbon composite			1204.7 mAh g^{-1} at 0.2 A g^{-1}	97% after 300 cycles at	70.9%	287.7 mAh g^{-1} at 5 A g^{-1}	[9]

				1 A g^{-1}			
Co organic frameworks@C	~1.5 mg cm^{-2}		1301 mAh g^{-1} at 0.1 A g^{-1}	98.6% after 2000 cycles at 10 A g^{-1}	60.6%	496 mAh g^{-1} at 20 A g^{-1}	[10]
CoO/C	~0.8~1.2 mg cm^{-2}		835.9 mAh g^{-1} at 0.2 A g^{-1}	118.6% after 300 cycles at 0.2 A g^{-1}	70.6%	400 mAh g^{-1} at 5 A g^{-1}	[11]
Fe_3O_4@C		91%	1204 mAh g^{-1} at 0.5 A g^{-1}	98.4% after 1000 cycles at 1 A g^{-1}	79%	606 mAh g^{-1} at 10 A g^{-1}	[12]
CNT@Co_3O_4	4 mg cm^{-2}	60%	957 mAh g^{-1} at 0.1 A g^{-1}	109% after 100 cycles at 0.1 A g^{-1}	74.8%	711 mAh g^{-1} at 1 A g^{-1}	[13]
MnO@C	1 mg cm^{-2}	79.6%	682 mAh g^{-1} at 0.1 A g^{-1}	100% after 1000 cycles at 0.5 A g^{-1}	59.9%	358 mAh g^{-1} at 5 A g^{-1}	[14]
CoO@ graphitic nanotubes		51%	1451 mAh g^{-1} at 0.1 A g^{-1}	83% after 80 cycles at 0.1 A g^{-1}	49.3%	247 mAh g^{-1} at 3 A g^{-1}	[15]
SnO_2/Graphene	3 mg cm^{-2}		1560 mAh g^{-1} at 0.1 A g^{-1}	93% after 100 cycles at 0.2 A g^{-1}	76.6%	360 mAh g^{-1} at 5 A g^{-1}	[16]
Carbon doped Co_3O_4	1 mg cm^{-2}		907 mAh g^{-1} at 0.5 A g^{-1}	104% after 300 cycles at 0.5 A g^{-1}	78.2%	853 mAh g^{-1} at 10 A g^{-1}	[17]
Porous current collector @Co_2VO_4@C			1140 mAh g^{-1} at 0.2 A g^{-1}	69% after 1000 cycles at 1 A g^{-1}		601 mAh g^{-1} at 20 A g^{-1}	[18]
MnO@C/rGO			791 mAh g^{-1} at 0.38 A g^{-1}	116% after 160 cycles at 0.38 A g^{-1}		562 mAh g^{-1} at 7.6 A g^{-1}	[19]
$CoFe_2O_4$@C		37.2%	858 mAh g^{-1} at 0.1 A g^{-1}	96% after 1000 cycles at 5 A g^{-1}	64.2%	306 mAh g^{-1} at 30 A g^{-1}	[20]

Binder-free GeO_2/reduced graphene	0.25 mg cm^{-2}	52%	1944 mAh g^{-1} at 0.2 A g^{-1}	59% after 500 cycles at 1 A g^{-1}	69%	845 mAh g^{-1} at 8 A g^{-1}	[21]
Binder-free Co-CoO_x nanowire array			925 mAh g^{-1} at 0.5 A g^{-1}	93% after 1000 cycles at 10 A g^{-1}	75%	568 mAh g^{-1} at 20 A g^{-1}	[22]
Binder-free CuO–Cu integrated anode	2.9 mg cm^{-2}		484 mAh g^{-1} at 0.8 A g^{-1}	86.7% after 800 cycles at 1.5 A g^{-1}	~35%	330 mAh g^{-1} at 2 A g^{-1}	[23]
Binder-free SnS_2 Nanosheet Arrays	1.8 mg cm^{-2}		1154 mAh g^{-1} at 0.1 A g^{-1}	78% after 500 cycles at 1 A g^{-1}	61.3%	639 mAh g^{-1} at 2 A g^{-1}	[24]
Binder-free Fe_3O_4/Carbon			754 mAh g^{-1} at 0.1 A g^{-1}	~80% after 100 cycles at 0.1 A g^{-1}	57%	410 mAh g^{-1} at 1 A g^{-1}	[25]
Binder-free Sn– and SnO_2–graphene		37%	793 mAh g^{-1} at 0.05 A g^{-1}	41.2% after 50 cycles at 0.05 A g^{-1}	51%	470 mAh g^{-1} at 2 A g^{-1}	[26]
Binder-free SnO_x-porous, carbon-nanofiber			828 mAh g^{-1} at 0.2 A g^{-1}	66.1% after 500 cycles at 0.2 A g^{-1}	65.1%	368 mAh g^{-1} at 2 A g^{-1}	[27]
Binder-free SnO_2 nanosheets	0.8 mg cm^{-2}		1196 mAh g^{-1} at 0.2 A g^{-1}	98% after 30 cycles at 0.2 A g^{-1}	75.8%	500 mAh g^{-1} at 0.2 A g^{-1}	[28]

[a] The cycling stability is calculated by Cn/Cs × 100% (Cn is the discharge capacity at the n cycle; Cs is the initial discharge capacity)

[b] Initial coulombic efficiency

Reference

(1) Wang, J.; Wu, J.; Wu, Z.; Han, L.; Huang, T.; Xin, H. L.; Wang, D. High-rate and long-life lithium-ion battery performance of hierarchically hollow-structured

NiCo2O4/CNT nanocomposite. *Electrochim. Acta* **2017,** *244*, 8-15.

(2) Liang, J.; Xi, K.; Tan, G.; Chen, S.; Zhao, T.; Coxon, P. R.; Kim, H.-K.; Ding, S.; Yang, Y.; Kumar, R. V. Sea urchin-like $NiCoO_2$@C nanocomposites for Li-ion batteries and supercapacitors. *Nano Energy* **2016,** *27*, 457-465.

(3) Rong, H.; Qin, Y.; Jiang, Z.; Jiang, Z.-J.; Liu, M. A novel NiCo2O4@GO hybrid composite with core-shell structure as high-performance anodes for lithium-ion batteries. *J. Alloy. Compd.* **2018,** *731*, 1095-1102.

(4) Fu, F.; Li, J.; Yao, Y.; Qin, X.; Dou, Y.; Wang, H.; Tsui, J.; Chan, K. Y.; Shao, M. Hierarchical NiCo2O4 Micro-/nanostructures with Tunable Morphologies as Anode Materials for Lithium- and Sodium-Ion Batteries. *ACS Appl. Mater. Inter.* **2017,** *9* (19), 16194-16201.

(5) Zhou, G.; Wu, C.; Wei, Y.; Li, C.; Lian, Q.; Cui, C.; Wei, W.; Chen, L. Tufted NiCo2O4 Nanoneedles Grown on Carbon Nanofibers with advanced electrochemical property for Lithium Ion Batteries. *Electrochim. Acta* **2016,** *222*, 1878-1886.

(6) Leng, J.; Wang, Z.; Li, X.; Guo, H.; Li, T.; Liang, H. Self-templated formation of hierarchical NiCo2O4 yolk-shell microspheres with enhanced electrochemical properties. *Electrochim. Acta* **2017,** *244*.

(7) Xin, H.; Li, D.; Shi, L.; Ji, M.; Lin, Y.; Yu, J.; Yang, B.; Li, C.; Zhu, C. A simple approach to fabricate of Ni-NiCo2O4@ZnCo2O4 yolk-shell nano-tetrahedron composite as high-performance anode material for lithium-ion batteries. *Chem. Eng.. J.* **2018,** *341*, 601-609.

(8) Wang, K.; Huang, Y.; Wang, M.; Yu, M.; Zhu, Y.; Wu, J. PVD amorphous carbon

coated 3D NiCo2O4 on carbon cloth as flexible electrode for both sodium and lithium storage. *Carbon* **2017,** *125*, 375-383.

(9) Li, M.; Du, H.; Kuai, L.; Huang, K.; Xia, Y.; Geng, B. Scalable dry-production of superior 3D net-like FeOx/C composite anode material for lithium ion battery. *Angew. Chem. Int. Edit.* **2017,** *56* (41), 12649-12653.

(10) Xiao, P.; Bu, F.; Zhao, R.; Aly Aboud, M. F.; Shakir, I.; Xu, Y. Sub-5 nm Ultrasmall Metal-Organic Framework Nanocrystals for Highly Efficient Electrochemical Energy Storage. *ACS Nano* **2018**.

(11) Wu, F.; Zhang, S.; Xi, B.; Feng, Z.; Sun, D.; Ma, X.; Zhang, J.; Feng, J.; Xiong, S. Unusual Formation of CoO@C "Dandelions" Derived from 2D Kagóme MOLs for Efficient Lithium Storage. *Adv. Energy Mater.* **2018**, 1703242.

(12) Liu, B.; Zhang, Q.; Jin, Z.; Zhang, L.; Li, L.; Gao, Z.; Wang, C.; Xie, H.; Su, Z. Uniform Pomegranate‐Like Nanoclusters Organized by Ultrafine Transition Metal Oxide@Nitrogen‐Doped Carbon Subunits with Enhanced Lithium Storage Properties. *Adv. Energy Mater.* **2018,** *8* (7), 1702347.

(13) Chen, Y.; Wang, Y.; Wang, Z.; Zou, M.; Zhang, H.; Zhao, W.; Yousaf, M.; Yang, L.; Cao, A.; Han, R. P. Densification by Compaction as an Effective Low‐Cost Method to Attain a High Areal Lithium Storage Capacity in a CNT@ Co3O4 Sponge. *Adv. Energy Mater.* **2018**, 1702981.

(14) Zhu, G.; Wang, L.; Lin, H.; Ma, L.; Zhao, P.; Hu, Y.; Chen, T.; Chen, R.; Wang, Y.; Tie, Z. Walnut‐Like Multicore–Shell MnO Encapsulated Nitrogen‐Rich Carbon Nanocapsules as Anode Material for Long‐Cycling and Soft‐Packed

Lithium‐Ion Batteries. *Adv. Functional Mater.* **2018,** *28* (18), 1800003.

(15) Tabassum, H.; Zou, R.; Mahmood, A.; Liang, Z.; Wang, Q.; Zhang, H.; Gao, S.; Qu, C.; Guo, W.; Guo, S. A Universal Strategy for Hollow Metal Oxide Nanoparticles Encapsulated into B/N Co‐Doped Graphitic Nanotubes as High‐Performance Lithium‐Ion Battery Anodes. *Adv. Mater.* **2018,** *30* (8), 1705441.

(16) Chen, W.; Song, K.; Mi, L.; Feng, X.; Zhang, J.; Cui, S.; Liu, C. Synergistic effect induced ultrafine SnO2/graphene nanocomposite as an advanced lithium/sodium-ion batteries anode. *J. Mater. Chem. A* **2017,** *5* (20), 10027-10038.

(17) Yan, C.; Zhu, Y.; Li, Y.; Fang, Z.; Peng, L.; Zhou, X.; Chen, G.; Yu, G. Local Built‐In Electric Field Enabled in Carbon‐Doped Co_3O_4 Nanocrystals for Superior Lithium‐Ion Storage. *Adv. Funct. Mater.* **2018,** *28* (7), 1705951.

(18) Zhu, C.; Liu, Z.; Wang, J.; Pu, J.; Wu, W.; Zhou, Q.; Zhang, H. Novel Co2VO4 Anodes Using Ultralight 3D Metallic Current Collector and Carbon Sandwiched Structures for High‐Performance Li‐Ion Batteries. *Small* **2017,** *13* (34).

(19) Liu, D.-H.; Lü, H.-Y.; Wu, X.-L.; Hou, B.-H.; Wan, F.; Bao, S.-D.; Yan, Q.; Xie, H.-M.; Wang, R.-S. Constructing the optimal conductive network in MnO-based nanohybrids as high-rate and long-life anode materials for lithium-ion batteries. *J. Mater. Chem. A* **2015,** *3* (39), 19738-19746.

(20) Zhang, L.; Wei, T.; Jiang, Z.; Liu, C.; Jiang, H.; Chang, J.; Sheng, L.; Zhou, Q.; Yuan, L.; Fan, Z. Electrostatic interaction in electrospun nanofibers: Double-layer carbon protection of $CoFe_2O_4$ nanosheets enabling ultralong-life and ultrahigh-rate lithium ion storage. *Nano Energy* **2018,** *48*, 238-247.

(21) Qiu, H.; Zeng, L.; Lan, T.; Ding, X.; Wei, M., In situ synthesis of GeO_2/reduced graphene oxide composite on Ni foam substrate as a binder-free anode for high-capacity lithium-ion batteries. *J. Mater. Chem. A* **2014,** *3* (4), 1619-1623.

(22) Zhan, L.; Wang, S.; Ding, L.-X.; Li, Z.; Wang, H., Binder-free Co–CoO_x nanowire arrays for lithium ion batteries with excellent rate capability and ultra-long cycle life. *J. Mater. Chem. A* **2015,** *3* (39), 19711-19717.

(23) Liang, P.; Zhang, H.; Su, Y.; Huang, Z.; Wang, C.-A.; Zhong, M., In situ preparation of a binder-free nano-cotton-like CuO–Cu integrated anode on a current collector by laser ablation oxidation for long cycle life Li-ion batteries. *J. Mater. Chem. A* **2017,** *5* (37), 19781-19789.

(24) Wang, J.-G.; Sun, H.; Liu, H.; Jin, D.; Zhou, R.; Wei, B., Edge-oriented SnS2 nanosheet arrays on carbon paper as advanced binder-free anodes for Li-ion and Na-ion batteries. *J. Mater. Chem. A* **2017,** *5* (44), 23115-23122.

(25) Wan, Y.; Yang, Z.; Xiong, G.; Luo, H., A general strategy of decorating 3D carbon nanofiber aerogels derived from bacterial cellulose with nano-Fe_3O_4 for high-performance flexible and binder-free lithium-ion battery anodes. *J. Mater. Chem. A* **2015,** *3* (30), 15386-15393.

(26) Botas, C.; Carriazo, D.; Singh, G.; Rojo, T., Sn– and SnO_2–graphene flexible foams suitable as binder-free anodes for lithium ion batteries. *J. Mater. Chem. A* **2015,** *3* (25), 13402-13410.

(27) Yan, F.; Tang, X.; Wei, Y.; Chen, L.; Cao, G.; Zhang, M.; Wang, T., Stannous ions reducing graphene oxide at room temperature to produce SnOx-porous,

carbon-nanofiber flexible mats as binder-free anodes for lithium-ion batteries. *J. Mater. Chem. A* **2015,** *3* (24), 12672-12679.

(28) Zhang, L.; Wu, H. B.; Lou, X. W., Growth of SnO_2 nanosheet arrays on various conductive substrates as integrated electrodes for lithium-ion batteries. *Mater. Horiz.* **2013,** *1* (1), 133-138.